Advanced Powder Technology 29 (2018) 2568–2581

Contents lists available at ScienceDirect

Advanced Powder Technology

journal homepage: www.elsevier.com/locate/apt

Original Research Paper

Numerical investigation of influence of treatment of the coke component on hydrodynamic and catalytic cracking reactions in an industrial riser

D.C. Pelissari [a], H.C. Alvares-Castro [b], J.L.G. Vergel [a], M. Mori [a,*]

[a] University of Campinas, School of Chemical Engineering, 500 Albert Einstein, Campinas, SP, Brazil
[b] Technological Units of Santander (UTS)/AC Ingenieria Virtual, Bucaramanga, Colombia

ARTICLE INFO

Article history:
Received 9 December 2017
Received in revised form 25 April 2018
Accepted 19 July 2018
Available online 31 July 2018

Keywords:
Riser
Fluid catalytic cracking
Numerical simulation
CFD

ABSTRACT

A three dimensional gas-solid reactive flow model based on the Eulerian-Eulerian approach was used to simulate the hydrodynamic, heat transfer and catalytic cracking reaction within in a conventional Fluid Catalytic cracking (FCC) riser. A 12-lump kinetic model was used to represent the catalytic cracking reaction network. It was proposed a catalyst deactivation model as a function of the weight percentage of coke amount on the catalyst to replace the deactivation model dependent of the residence time. It was compared the effects of novel treatment for coke component (coke produced in the solid phase) with common treatment (coke produced in the gas phase) on the fluid dynamic and catalytic cracking. The results showed that the treatment for coke component affects radial distribution of coke mass flow. It also showed that the treatment for coke plays an important role in simulation with catalyst deactivation as a function of coke amount on catalyst.

1. Introduction

The worldwide increase in demand for petroleum products, combined with the increase in the supply of low-grade crude oil, has forced the refineries to use chemical process to refine the atmospheric residue and vacuum gas oil of distillation [1,2]. In this context, the fluid catalytic cracking (FCC) process has been highlighted, and it is estimated that 45% of the world's gasoline comes from this process [3–5]. According to Fahim et al. [6], in the FCC unit, the heavy oil fractions of low commercial value are converted into products with higher added value, mainly gasoline and diesel, through the contact between the feedstock and catalyst in a fluidized bed regime. In addition, it stands out for its flexibility, adjusting the profile of the products to the market demand, through the control of the operational variables.

Among the several equipment in the FCC unit, it is in the reactor, called a riser, that the initial contact between the gasoil and the catalyst occurs, and consequently the catalytic reactions. The riser is described as a cylinder with a high height/diameter ratio, which aims to promote the contact between the feedstock and the catalyst for a specific time. The phenomena that occur within the riser are extremely complex, due to the heterogeneous reactions, mass, momentum and energy transfer between the phases, catalyst deactivation by coke deposition and volumetric expansion. Furthermore, the riser operates at high temperature and pressure, which makes the experimental study in an industrial riser unachievable [7].

In this context, to overcome the lack of knowledge about this important process, researchers have used computational fluid dynamics (CFD) as a tool to predict and analyze the phenomena that occur in this kind of flow. As a result, a wide range of studies using CFD and different kinetics model have been conducted to improve FCC riser performance from analysis of different geometries and operating conditions. Theologos et al. [8] studied the influence of the number of nozzles on the fluid dynamics and the gasoline yield. They used an Eulerian-Eulerian approach applied in a 3D gas-solid flow and a 10-lump kinetic model. The simulations results showed that increasing the number of nozzles from four to twelve increased the gasoline yield by 4%, since it provide a more uniform catalyst distribution. Lopes et al. [9] simulated the FCC riser using a 3-D three-phase model and 4-lump kinetic model. In their work, it was studied the influence of the geometry of the riser outlet on the flow and products yield. It was observed that small changes in the riser outlet configuration have a significant effect on the process. An increase in gasoline yield was observed with increasing reactive mixture residence time. However, in their kinetic model the gasoline does not crack, in this

* Corresponding author.
E-mail address: mori@feq.unicamp.br (M. Mori).

https://doi.org/10.1016/j.apt.2018.07.012
0921-8831/

Nomenclature

C_i	molar concentration of component I [kmol m^{-3}]
C_D	drag coefficient [–]
C_μ	constant 0.09
$C_{\in,1}$	constant 1.44
$C_{\in,2}$	constant 1.92
d	particle diameter [m]
g	gravitational acceleration [m^2 s^{-1}]
G	elasticity modulus [Pa]
G_0	constant of elasticity modulus function [Pa]
H	static enthalpy [J mol^{-1}]
k	turbulent kinetic energy [m^2 s^{-2}]
m_{coke}	reaction rate of coke in the solid phase [kg m^{-3} s^{-1}]
Nu	Nusselt number [–]
p	static pressure [Pa]
p^k	shear production of turbulence [Pa s^{-1}]
Pr	Prandtl number [–]
R_i	reaction rate of component i [kg m^{-3} s^{-1}]
Re	Reynolds number [–]
t	time [s]
T	static temperature [K]
$\boldsymbol{u}$	velocity vector [m s^{-1}]
Y_{coke}	mass fraction of coke [–]
Y_i	mass fraction of component i [–]

Greek symbols

β	interphase momentum transfer [kg m^{-3} s^{-1}]
ε	volume fraction [–]
$\in$	turbulence dissipation rate [m^2 s^{-3}]
γ	interphase heat transfer coefficient [W m^{-2} K^{-1}]
λ	thermal conductivity [W m^{-1} K^{-1}]
μ	viscosity [Pa s]
ρ	density [kg m^{-3}]
σ_k	constant 1.00
$\sigma_\in$	constant 3.00

Subscripts

g	gas phase
lam	laminar
r	reaction
s	solid phase
turb	turbulent

way, longer residence times increase the gasoline yield. Behjat et al. [10] conducted a 3D reactive three-phase-flow numerical experiment, including feedstock coalescence and vaporization, to evaluate the influence of the number of nozzles on the riser fluid dynamics and heat transfer. The results showed that the increase in the number of nozzles improved the catalyst distribution, a result that corroborates those of Theologos et al. [8]. Chang et al. [3] simulated an industrial riser using a 12-lumps kinetic model and considering the vaporization phenomenon. The results of the simulation showed that the decrease in the nozzle angle increases the feedstock conversion and coke yield, while the decreasing the yield of diesel and gasoline. Li et al. [11] analyzed the effects of nozzle jet velocity, nozzle position and nozzle angle. The nozzle jet velocity played a significant role on the gas-solid flow. Regarding the nozzle position, it was not observed significant effects on the fluid dynamic profile or on the riser efficiency. It was observed that nozzle angle had significant effect on the radial temperature distribution and gasoline yield. The catalyst-to-oil ratio was studied by Nayak et al. [12], Chang et al. [3] and Alvarez-Castro et al. [4]. It was observed an increase in the conversion with the increase of catalyst-to-oil rate. Regarding the gasoline, the three works diverged. Nayak et al. [17] reported an increase in gasoline yield with the increase of catalyst-to-oil rate, whereas Chang et al. [3] and Alvarez-Castro et al. [4] reported no significant effect and decrease in gasoline yield, respectively. Alvarez-Castro et al. [4] also evaluated the influence of catalyst inlet temperature. The authors observed that increasing the temperature decreases the gasoline and diesel yield, while increases the conversion and the yield of coke, LPG and dry gases.

As previously seen, several studies are conducted to obtain better yield and understand better the phenomena that occur in the FCC process due to its importance. However, such research is only possible with the development of both fluid dynamic and kinetics models, capable of predicting the phenomena that occur within the riser. The modeling of the reactions that occur in the riser is not a trivial task, due to the high number of components present and, consequently, to the high number of reactions that occur in this process. In this context, several approaches have been developed to represent the kinetics of catalytic cracking reactions. Among the different approaches found in the literature, the most used one was developed by Weekman and Nace [13] and called "lumps," in which petroleum components that have similar properties and behaviors (molecular weight, boiling point, number of carbons) are grouped into pseudo-components (lumps). In the Weekman and Nace [13] model all reactions are represented by the kinetics of three chemical species (gasoil, gasoline and other products).

As the composition of gasoil can vary depending on the petroleum, models such as those by Weekman and Nace [13], in which the feedstock is represented by a single lump, make it necessary to estimate the kinetic constants for each type of feedstock. Considering this, Jacob et al. [14] proposed a 10-lump model in which gasoil is divided according to its chemical characteristics into 4 lumps (aromatic, aromatics with substituents, naphthenic, and paraffinic), in which the dependence of the kinetic parameters, according to the feedstock composition, is considered.

Due to the different demands of petroleum products and the different types of petroleum, different catalytic cracking processes were proposed. Yang et al. [7] reported some of them in their work, such as the maximizing iso-paraffin in cracked naphtha (MIP) process and flexible dual-riser fluid catalytic cracking (FDFCC). Thus, from the models by Weekman and Nace [13] and Jacob et al. [14] other models have been proposed to fulfill the deficiencies of previous models or to meet the needs of their project. As a result, kinetic models of different lumps have been proposed (3-lumps [13], 5-lumps [14], 6-lumps [15], 10-lumps [16,17], 14-lumps [18]). In addition to the different numbers of lumps, the kinetics models also differ, considering different mechanisms, such as gasoline cracking, catalyst deactivation type, deactivation by basic nitrogen poisoning and absorption of aromatic, and asphaltenic resins.

Deactivation of the catalyst is another important factor that must be considered in the kinetic modeling of reactions. The deposition of coke on the catalyst surface lowers the activity thereof. The literature shows two main models to represent the catalyst deactivation: as a function of residence time and as a function of coke concentration. Cerqueira et al. [19] used the 12-lump model to evaluate different functions to describe the catalyst deactivation, and they observed that an exponential function with only one variable parameter generates satisfactory results. Depending

on the type of catalyst and process, several parameters of the deactivation function can be found.

In the literature, both the deactivation models, as a function of the residence time and as a function of the percentage of coke, are quite used and represent, in a satisfactory way, the catalyst deactivation. However, according to Guinest and Ribeiro [20], deactivation functions, such as the catalyst residence time, do not have direct connection with the operating conditions (pressure, temperature), leading to imprecise predictions of the catalyst activity along the reactor. Thus, a more reliable description of the decay of the catalyst activity can be obtained when the deactivation model is expressed as a function of the variable that causes its deactivation, in this case, the coke deposited on the catalyst.

It is noteworthy that all the kinetic models and works cited, as well as most of the works found in the literature, consider coke formation in the gas phase, which does not occur in the industrial process. Nevertheless, Yang et al. [7] included in their modeling the coke formation in the solid phase and used 11-lumps kinetic model with catalyst deactivation as function of the mass fraction of coke deposited on catalysts to simulate the FCC process. It was suggested that this novel treatment for coke component is more realistic, since the coke was formed in the catalyst. However, those authors did not compare the treatments given to coke, whether formed in the gas phase (common treatment) or in the solid phase (new treatment), making it impossible to observe the effects and relevance that the type of treatment given to coke have on the profile flow, coke distribution at the riser, and kinetics.

In the present work, a three-dimensional reactive gas-solid flow based on Eulerian-Eulerian approach was used to investigate fluid dynamic, heat transfer and catalytic cracking reaction in an industrial scale FCC riser. The 12-lumps kinetic model was incorporated into the CFD model, which has a catalyst deactivation model as function of the catalyst residence time. It was proposed a catalyst deactivation model as a function of the weight percentage of coke amount on the catalyst in order to replace the deactivation model dependent of the residence time, since in the real process the deactivation occurs due to the coke deposition on the catalyst. It was compared the effects of novel treatment for coke component given by Yang et al. [7] with the common treatment (coke produced in the gas phase) on the fluid dynamic and catalytic reactions. This comparison was performed for two types of catalyst deactivation function (by residence time and weight percentage coke). The results were compared with the industrial data reported by Chang et al. [3].

2. Mathematical model

A three-dimensional reactive flow based on the Eulerian-Eulerian approach was used to describe the gas-solid flow of the FCC riser. In Eulerian-Eulerian approach both the phases are considered to be continuous and interpenetrating, in which the conservation equations for mass, momentum, species, and energy are solved for each phase and simultaneously, as shown in Table 1. The catalytic cracking reactions were represented by 12-lumps kinetic model [21]. The momentum equations of each phase are linked by an interphase exchange term. This term is calculated through the drag laws, since the drag force between the fluid phase and the dispersed phase is one of the dominant forces in fluidized beds [22]. Several drag models are found in the literature to represent the gas-solid flow, as the models of Gidaspow [23], Syamlal and O'Brien [24] and Yang et al. [25]. It was used the drag model based on the energy minimization multiscale (EMMS) approach proposed by Yang et al. [25]. The modulus of elasticity (G) given by Gidaspow [23] in Eq. (19) was used to predict the solid pressure. The k-ϵ two-equation model was used to predict gas-phase effective turbulence viscosity. In the gas energy equation, Eq. (5), the last two terms are the energy variation due to the endothermic reactions and the heat transfer between the phases, respectively. The interphase heat transfer coefficient, h, is related to the Nusselt number, which is calculated by the Ranz-Marshall [26,27] correlations. It was assumed that feedstock was completely vaporized at the feedstock inlet, since the required time for the complete vaporization of the feedstock is approximately 3% (0.3–30 ms) of the mixture residence time in the typical FCC riser [7,11,22,28].

2.1. Catalytic cracking kinetic model

It was used the 12-lumps kinetic model by Wu and Weng [21] to represent the catalytic cracking reactions. In this model, the feedstock and products are divided into three and nine lumps, respectively, listed in Table 2, and the reaction scheme is represented by 56 reactions, shown in Fig. 1. The reaction paths and kinetic parameters are shown in Table 3. It was assumed that all reactions are first-order and irreversible, and catalyst deactivation is unselective. The term R_i, in Eq. (7), is the sum of rates of formation and consumption of specie i, being the reactions rates ($r_{i,r}$) expressed as below:

$$r_{r,i} = -\phi(C)\cdot \mathrm{F}(N)\cdot \mathrm{F}(A)\cdot \mathrm{k_r}\cdot\left(\rho_g\alpha_i\right)\cdot\rho_s\varepsilon_s \tag{22}$$

$$\mathrm{k_r} = k_0\cdot\exp\left(\frac{-E}{RT}\right) \tag{23}$$

$$\phi(C) = \exp(-0.2543t) \tag{24}$$

$$\mathrm{F(A)} = \frac{1}{1+K_A(C_A+C_R)} \tag{25}$$

$$\mathrm{F(N)} = \frac{1}{1+K_N C_N} \tag{26}$$

where ($\rho\alpha_i$) is the mass concentration of the reactant i in the gas phase, ($\rho_s\varepsilon_s$) is the local concentration of the catalyst, k_r is the reaction constant, k_0 is the pre-exponential factor, and E is the activation energy. Φ(C), F(A) and F(N) are the catalyst deactivation function due to the coke deposition which is calculated as a function of catalyst residence time, polycyclic aromatic adsorption and basic nitrogen poisoning, respectively. The terms C_A, C_R and C_N are the weight percentage of aromatics, resins and asphaltene and nitrogen in feedstock. K_A and K_N are the adsorption coefficient of heavy aromatics compounds and the coefficient of deactivation of basic nitrogen poisoning.

The heat of cracking reactions, Q_r in Eq. (5), is calculated according to the mass of coke produced [3,7,11]. It is reported that the cracking reactions in FCC process are endothermic reactions, and producing 1 kg coke requires the amount of heat of 9.127×10^3 kJ. Thus, Q_r is equal to 9.127×10^3 kJ multiplied by the rate of coke formation rate.

One of the main objectives of this work was to implement a catalyst deactivation model as a function of the weight percentage of coke on amount of catalyst. Thus, it was used a similar function to one that considers the residence time, as shown in Eq. (27). The term A_0 is used to adjust catalyst activity due to change in formulation, α' is the deactivation constant and C is the weight percentage of coke on amount of catalyst [29].

$$\phi(C) = A_0 e^{(-\alpha' C)} \tag{27}$$

To obtain the values of the constants in Eq. (27), it was taken the values of the catalyst residence time and the weight percentage of coke along the height of the riser from the simulation result using the Wu and Weng [21] model, which was used in Eq. (24) e Eq.

Table 1
Governing and constitutive equations for gas-solid flow.

Governing equations	
Continuity equations of gas and solid phases	
$\frac{\partial}{\partial t}\left(\varepsilon_g \rho_g\right) + \cdot\left(\varepsilon_g \rho_g \boldsymbol{u}_g\right) = -m_{coke}$	(1)
$\frac{\partial}{\partial t}(\varepsilon_s \rho_s) + \cdot(\varepsilon_s \rho_s \boldsymbol{u}_s) = m_{coke}$	(2)
Momentum equations of gas and solid phases	
$\frac{\partial}{\partial t}\left(\varepsilon_g \rho_g \boldsymbol{u}_g\right) + \cdot\left(\varepsilon_g \rho_g \boldsymbol{u}_g \boldsymbol{u}_g\right) = \cdot\left[\varepsilon_g \mu_g \left(\boldsymbol{u}_g + (\boldsymbol{u}_g)^T\right)\right] - \varepsilon_g p + \varepsilon_g \rho_g \boldsymbol{g} + \beta(\boldsymbol{u}_s - \boldsymbol{u}_g)$	(3)
$\frac{\partial}{\partial t}(\varepsilon_s \rho_s \boldsymbol{u}_s) + \cdot(\varepsilon_s \rho_s \boldsymbol{u}_s \boldsymbol{u}_s) = \cdot\left[\varepsilon_s \mu_s \left(\boldsymbol{u}_s + (\boldsymbol{u}_s)^T\right)\right] - \varepsilon_s \mathrm{G} \varepsilon_s + \varepsilon_s \rho_s \boldsymbol{g} + \beta(\boldsymbol{u}_g - \boldsymbol{u}_s)$	(4)
Energy equation of gas and solid phases	
$\frac{\partial}{\partial t}\left(\varepsilon_g \rho_g H_g\right) + \cdot\left(\varepsilon_g \rho_g \boldsymbol{u}_g H_g\right) = .[\varepsilon_g \lambda_g T_g] - Q_r + h_{gs}(T_s - T_g)$	(5)
$\frac{\partial}{\partial t}(\varepsilon_s \rho_s H_s) + \cdot(\varepsilon_s \rho_s \boldsymbol{u}_s H_s) = .[\varepsilon_s \lambda_s T_s] + h_{gs} A_{g/s}(T_g - T_s)$	(6)
Species transport equation of gas phase and	
$\frac{\partial}{\partial t}\left(\varepsilon_g \rho_g Y_{i,g}\right) + \cdot\left(\varepsilon_g \rho_g u_g Y_{i,g}\right) = .\left(\varepsilon_g \rho_g \Gamma_i Y_{i,g}\right) + R_i$	(7)
Species transport equation for coke in catalyst phase.	
$\frac{\partial}{\partial t}(\varepsilon_s \rho_s Y_{coke}) + \cdot(\varepsilon_s \rho_s u_s Y_{coke}) = .(\varepsilon_s \rho_s \Gamma_{coke} Y_{coke}) + m_{coke}$	(8)
Turbulence Equation ($k - epsilon$ model)	
$\mu_g = \mu_{lam,g} + \mu_{turb,g}$	(9)
$\mu_{turb,g} = \rho_g C_\mu \frac{k^2}{\epsilon}$	(10)
$\frac{\partial}{\partial t}\left(\varepsilon_g \rho_g k\right) + \cdot\left(\varepsilon_g \rho_g \boldsymbol{u}_g k\right) = \cdot\left[\varepsilon_g \left(\mu_{lam,g} + \frac{\mu_{turb,g}}{\sigma_k}\right) k\right] + \varepsilon_g P^k - \varepsilon_g \rho_g \epsilon$	(11)
$\frac{\partial}{\partial t}\left(\varepsilon_g \rho_g \epsilon\right) + \cdot\left(\varepsilon_g \rho_g \boldsymbol{u}_g \epsilon\right) = \cdot\left[\varepsilon_g \left(\mu_{lam,g} + \frac{\mu_{turb,g}}{\sigma_\epsilon}\right) \epsilon\right] + \frac{\varepsilon_g \epsilon}{k}\left(C_{\epsilon,1} P^k - C_{\epsilon,2} \epsilon \rho_g\right)$	(12)
$P^k = \mu_{turb,g} \boldsymbol{u}_g \cdot \left(\boldsymbol{u}_g + (\boldsymbol{u}_g)^T\right)$	(13)
Drag Forc	
$\beta = \begin{cases} 150 \frac{\varepsilon_s^2 \mu_g}{\varepsilon_g d_s^2} + \frac{7}{4} \frac{\lvert \boldsymbol{u}_s - \boldsymbol{u}_g \rvert \varepsilon_s \rho_g}{d_s} \varepsilon_g < 0.74 \\ \frac{3}{4} C_D \frac{\lvert \boldsymbol{u}_s - \boldsymbol{u}_g \rvert \varepsilon_s \varepsilon_g \rho_g f(\varepsilon_g)}{d_s} \varepsilon_g \geq 0.74 \end{cases}$	(14)
$f(\varepsilon_g) = -0.576 + \frac{0.0214}{4(\varepsilon_g - 0.7463)^2 + 0.0044} 0.74 \leq \varepsilon_g \leq 0.82$	(15)
$f(\varepsilon_g) = -0.0101 + \frac{0.0038}{4(\varepsilon_g - 0.7789)^2 + 0.0040} 0.82 < \varepsilon_g \leq 0.97$	(16)
$f(\varepsilon_g) = -31.8295 + 32.8295 \varepsilon_g \varepsilon_g > 0.97$	(17)
$C_D = \begin{cases} 0.44 Re_s > 1000 \\ \frac{24}{Re_s}\left[1 + 0.15 (Re_s)^{0.687}\right] Re_s < 1000 \end{cases}$	(18)
Solid Pressure	
$G = G_0 \exp\left[c(\varepsilon_s - \varepsilon_{s,max})\right]$	(19)
Heat transfer coefficient between phases	
$h_{gs} = \frac{\lambda_g Nu}{d_p}$	(20)
Ranz-Marshall Correlation	
$Nu = 2.0 + 0.6 Re^{0.5} Pr^{0.33}$	(21)

Table 2
Lumps of the kinetic model by Wu and Weng [21].

Symbol	Lump	Boiling range
S_S	Saturates in feedstock	613.15 K+
S_A	Aromatics in feedstock	
S_R	Resin and asphaltene in feedstock	
D_I	Diesel	477.15–613.15 K
G_S	Saturates in gasoline	C_5 – 477.15 K
G_O	Oleofins in gasoline	
G_A	Aromatics in gasoline	
L_P	Low carcon alkanes	$C_3 - C_4$
L_{O3}	Propylene	
L_{O4}	Butene	
D_R	Dry gas	$C_1 + C_2 + H_2$
C_K	Coke	–

(27). Thus, Rstudio software was used to minimize the square sum of the difference between the equations. The values obtained for A_0 and α' were 0.9 and 0.853, respectively.

3. Simulation

In this work, it was used the same riser geometry reported by Chang et al. [3]. The selected riser is 41.3 m in height and 1.05 m in diameter, as shown in Fig. 2. The catalyst and steam were fed at the bottom of the riser. The steam is a fluidization agent, which is used to drag the catalyst to the injection zone, located at the height of 1.5 m above the reactor base. In this zone, there are four nozzles evenly distributed around the riser with an angle of 60° with the horizon, which are used to feed the gas oil into the riser.

In order to validate the simulation, it was used the operating condition reported by Chang et al. [3]. It was assumed that feedstock is introduced at vaporization temperature (733 K), a value reported in the literature [7]. Chang et al. [3] considered the phenomenon of vaporization of the feedstock. Thus, the energy required to vaporization of the feedstock was deducted from the initial temperature of the catalyst. Being it was adopted the same procedure used by Lopes [30]. The non-slip condition was set for gas phase and free slip condition for the solid phase. The operation and boundary conditions are listed in Table 4. In addition, the physical properties of the reactive species, the catalyst and steam are listed in Table 5.

The commercial software Workbench 14.0 was used to create the geometry and mesh, which was imported into the ANSYS CFX 14.0. The differential equations were solved using the finite volume method. A second-order upwind scheme was applied to calculate conservation equations, while the turbulence term was calculated by first-order upwind scheme. The temporal discretization was estimated via the second-order backward Euler method. The terms of catalytic reactions rate, heat of reactions, transfer of mass, and drag model were implemented as source terms in the

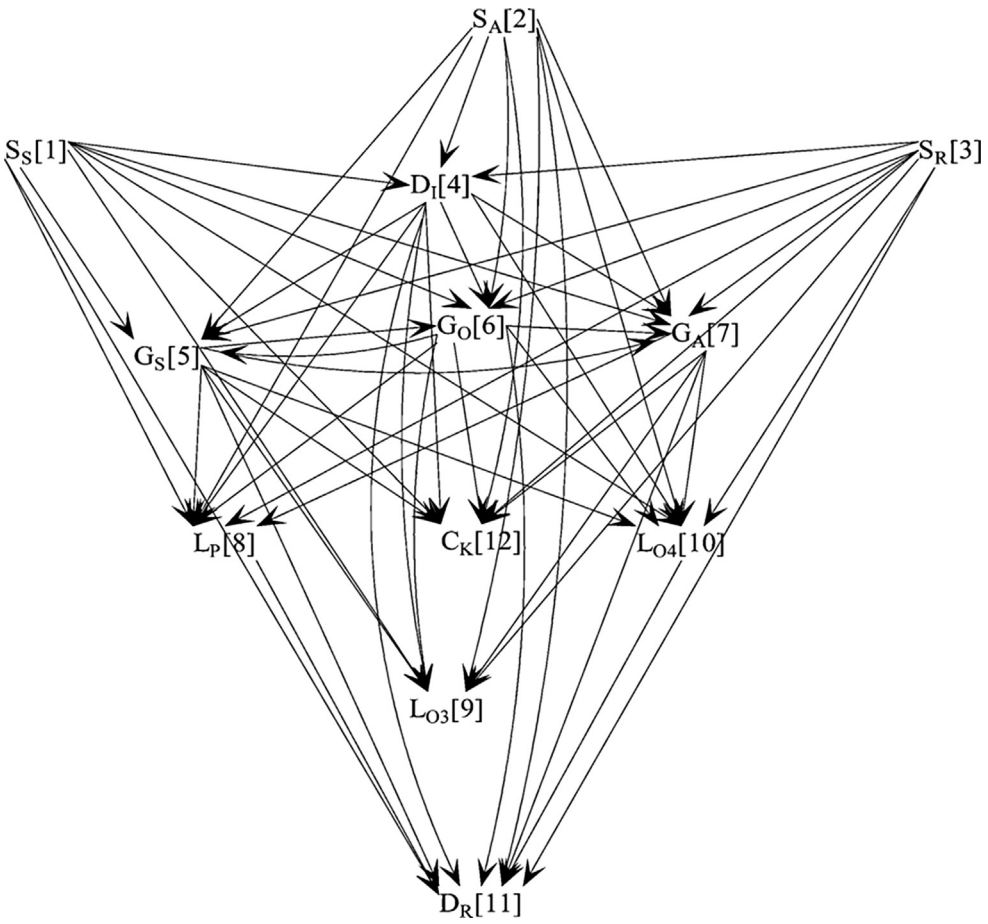

Fig. 1. Reaction network of the 12-lump kinetic model.

Table 3
Kinetics parameters of the 12-lumps kinetic model.

Reaction Path	Activation energy (kJ/mol)	Exponential factor (m^3/kg/s)	Reaction Path	Activation energy (kJ/mol)	Exponential factor (m^3/kg/s)
1 → 4	2.7251	0.8309	4 → 6	13.0832	0.05712
1 → 5	0.9432	0.1705	4 → 7	12.2401	0.2716
1 → 6	1.2912	0.8854	4 → 8	8.2513	0.02983
1 → 7	7.2956	0.0516	4 → 9	3.7156	0.005163
1 → 8	13.03682	0.0160	4 → 10	3.4688	0.008104
1 → 9	8.9495	0.0320	4 → 11	16.3068	0.09068
1 → 10	7.7870	0.0094	4 → 12	10.2884	0.2953
1 → 11	8.8766	0.01116	5 → 6	14.641	0.01762
1 → 12	9.5764	0.009691	5 → 7	15.7166	0.06452
2 → 4	4.7964	1.0488	5 → 8	15.3998	0.000109
2 → 5	4.0451	0.1679	5 → 9	13.124	0.07185
2 → 6	14.1004	0.1510	5 → 10	12.8934	0.2853
2 → 7	13.5735	0.2189	5 → 11	18.2895	0.08753
2 → 8	0.7088	0.04371	5 → 12	19.805	0.01101
2 → 9	3.4203	0.09726	6 → 5	12.6572	0.04536
2 → 10	3.7921	0.04795	6 → 7	8.9658	0.4008
2 → 11	4.7483	0.04531	6 → 8	13.5233	9.70E-13
2 → 12	3.3867	0.07244	6 → 9	12.1083	0.1863
3 → 4	10.1081	0.1928	6 → 10	12.1945	0.1563
3 → 5	14.3479	0.2450	6 → 11	14.6554	0.1371
3 → 6	15.8237	1.1487	6 → 12	11.3696	0.04921
3 → 7	16.0157	0.1235	7 → 8	14.0169	1.14E-5
3 → 8	0.9537	0.3900	7 → 9	11.9348	0.09565
3 → 9	1.9214	0.1617	7 → 10	10.4221	0.4191
3 → 10	1.35212	0.1076	7 → 11	10.2512	0.4263
3 → 11	4.0009	0.1039	7 → 12	9.3636	0.2278
3 → 12	3.9143	0.1169	8 → 11	30.3051	0.2538
4 → 5	14.4455	0.06207	10 → 11	38.5004	0.2344

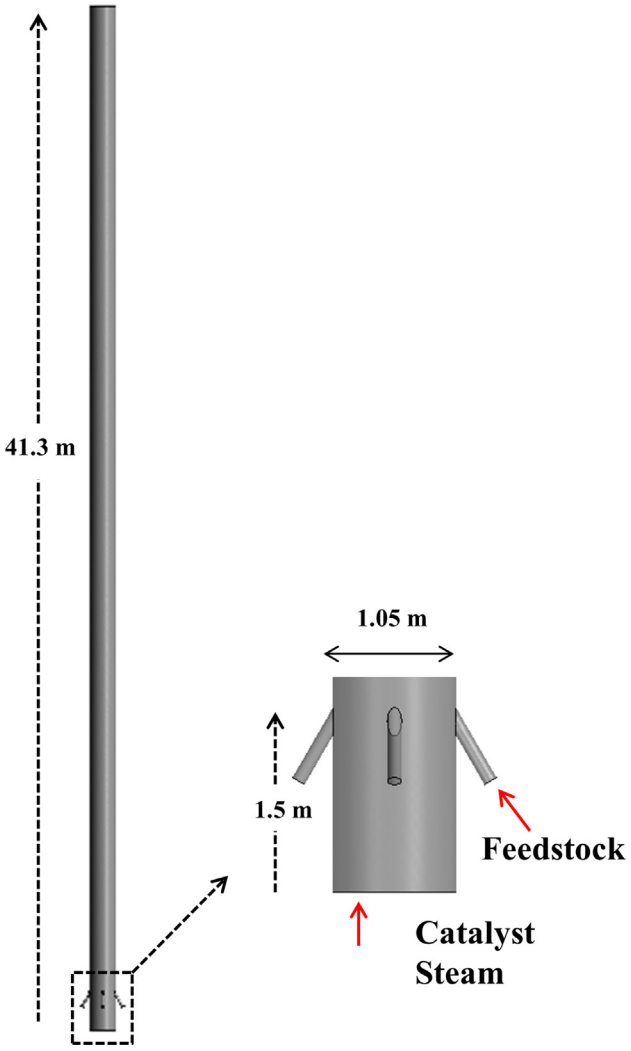

Fig. 2. Riser geometry.

Table 4
Operation and boundary conditions.

Inlet of Catalyst and steam	
Boundary condition	*Inlet*
Velocity	5 m/s
Temp. of catalyst	868 K
Temp. of steam	868 K
Vol. fraction of catalyst	0.042
Vol. fraction of steam	0.958
Inlet of feedstock	
Boundary condition	*Inlet*
Flux of feedstock	34.57 kg/s
Temp. of feedstock	733 K
Vol. fraction of catalyst	0
Vol. fraction of feedstock	1
Mass fraction of feedstock	
Saturetes	0.6605
Aromactics	0.2525
Resin and asphaltenes	0.087
Oultlet	*Openning*
Wall	*Free slip* para fase sólida e *no-slip* para fase gás

conservation equations of continuity, momentum, species, and energy by means of user defined functions (UDFs). A time step of 1 ms was used to guarantee the numerical convergence. The amount of time required for the simulations was defined based on the stabilization of the outlet mass fraction of gasoline, diesel, LPG, and dry gas. The total time of simulation was 15 s, similar time reported by Alvarez-Castro et al. [4], Lopez et al. [9] and Alvarez-Castro et al. [31].

4. Results

4.1. Hydrodynamic behavior

The volume fraction profile of the catalyst in the axial plane and the cross-section planes at different heights are shown in Fig. 3. It can be observed that in injection zone (1.45 and 2.5 m), part of the catalyst is directed towards the center of the riser due to the high velocity injection of the feedstock, while the other part tends to accumulate near the wall. At the height of about 4.0 m, the solid phase is concentrated in the center region. Along the height of the riser, it can be noted that the volume fraction of the catalyst tends to reduce and homogenize due to the acceleration and volumetric expansion of the gas phase caused by the formation of low molecular weight products.

Fig. 4 shows the profile and vector of the gas phase velocity in axial plane. The injection zone is the most difficult region to describe, since there are high gradients of velocity and concentration. In this region, the feedstock is injected at high velocity from nozzle towards the riser center. After entering in the riser, the gasoil collides with a large amount of catalyst coming from the bottom of the riser. Thus the catalyst is directed to the center and a preferred path for the passage of the feedstock is formed. It can be observed in this region, Fig. 4(a), a slower velocity both in the center and near the wall of the riser, where there is high concentration of solid, whereas a high velocity is observed between these two regions due to the fast injection of gas oil. The same behavior is reported by other researchers [3,7].

It can be seen a rapid reduction in gas velocity right after its injection due to the expansion of the flow space and the momentum transfer between the gas and solid phase. Along the riser height, the heavy oil is cracked in light fractions of petroleum, causing volumetric expansion of gas phase and consequently an increase in its velocity, as show in Fig. 4. Above the injection zone, the gas phase concentrates in the center region while the solid phase concentrated near the wall, resulting in a high velocity in the riser center, as shown in Fig. 4(b) and (c). Moreover, the results indicate that velocity is not uniform in axial and radial directions, mainly in the injection zone.

4.2. Temperature profile

Fig. 5 shows the gas phase temperature profile in axial plane. The heat transfer phenomena and reaction rate are closely related to the catalyst distribution, and as previously discussed, the radial and axial velocity and catalyst distribution are not uniform, mainly in the injection zone. Thus, it can be observed the similar temperature profile to the catalyst distribution in Fig. 3, in which the highest temperature occurs in the center and near the wall, where there is high concentration of solid. It is also noted that the heat transfer rate from catalyst to the feedstock is elevated. Along at the riser height, the temperature decrease due to the endothermic catalytic reactions.

4.3. Species concentration profiles

Fig. 6 shows the feedstock conversion and the yield of various products along the riser height. It can be noted that feedstock is rapidly cracked in the first one-third of the riser, due to the higher

Table 5
Physical properties of reactive species, catalyst and steam.

Species	Molecular weight (kg/kmol)	Specific mass (kg/m^3)	Specific heat (J/kg K)	Viscosity (kg/m s)	Thermal conductivity (W/m K)
S_S	420	14.52	2420	$5 * 10^{-5}$	0.0250
S_A	420	14.52	2420	$5 * 10^{-5}$	0.0250
S_R	420	14.52	2420	$5 * 10^{-5}$	0.0250
D_I	240	8.6	2420	$1.6 * 10^{-5}$	0.0250
G_S	117	4.2	2420	$1.6 * 10^{-5}$	0.0250
G_O	117	4.2	2420	$1.6 * 10^{-5}$	0.0250
G_A	117	4.2	2420	$1.6 * 10^{-5}$	0.0250
L_P	50	1.76	2420	$1.6 * 10^{-5}$	0.0250
L_{O3}	50	1.76	2420	$1.6 * 10^{-5}$	0.0250
L_{O4}	50	1.76	2420	$1.6 * 10^{-5}$	0.0250
D_R	18.4	0.8	2420	$1.6 * 10^{-5}$	0.0250
C_K	400	1400	1090	$1.6 * 10^{-5}$	0.0250
Catalyst	–	1560	1090	$1.72 * 10^{-5}$	0.0454
Steam	18.02	0.6	2080.1	$1.22 * 10^{-5}$	0.0250

temperature, concentration of reactant and concentration of catalyst. The yield of diesel and total gasoline increase quickly in the first half of the riser, and after approximately keep stable. It can be observed that olefins in gasoline increases rapidly, reaches maximum and then decline gradually, while the saturates and aromatics in gasoline increase gradually along the height of the riser. The concentration of LPG, dry gases and coke increase progressively along the riser.

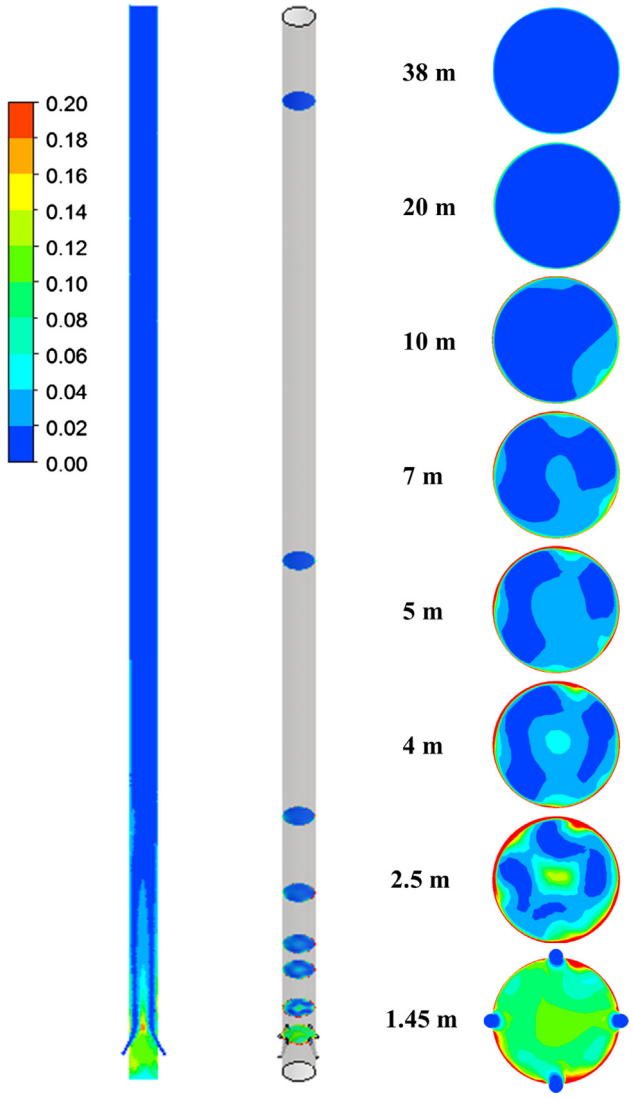

Fig. 3. Catalyst volume fraction contour profiles in the axial and radial planes.

4.4. Effect of treatment of coke component

Yang et al. [7] suggested that the novel treatment for coke, which is incorporated in the catalyst phase, is more realistic since in the real process it occurs in this way. Thus, the simulation comprises four cases, i.e. simulating the coke production in solid phase and gas phase using the deactivation of catalyst as a function of residence time (cases 1 and 2. respectively) and simulating the coke production in solid phase and gas phase using the deactivation of catalyst as a function of weight percentage of coke (cases 3 and 4, respectively).

In cases 1 and 3, in which the coke is produced in the solid phase, we used the same procedure used by Yang et al. [7]. Thus, a term of source for mass transfer between the phases was incorporated into the simulation, which is equal to the sum of the reaction rates of the coke formation. In the simulation, the gas phase is composed of steam and the lumps of Tab. 2, except for coke. The dispersed phase is considered a mixture composed of the catalyst and the coke.

In cases 2 and 4, in which the coke is produced in the gas phase, we used the same procedure used by Chang et al. [3], Alvarez-Castro et al. [31]. The gas phase is composed of steam and the lumps of Tab. 2. The dispersed phase is composed of the catalyst.

4.4.1. Effect of different treatment for coke on hydrodynamic

Fig. 7 shows the volume fraction of the catalyst, mass flow of the coke and weight percentage of the coke amount on catalyst in cross-section at 25 m in height. The effects of treatment of coke on hydrodynamic were similar for both deactivation model, thus, for illustration, the results showed in Fig. 7 refers to the case 1 and case 2. The volume fraction of solid phase is similar for both cases, with a dense region near the wall and a diluted region in the center. The production of coke is favored by the accumulation of catalyst, which causes high temperature regions. Consequently it is expected that there is higher amounts of coke in regions with high concentration of catalyst. This can be observed for case 1, in which the mass flow of coke is higher near the wall, whereas in case 2 (common treatment for coke) a uniform mass flow of coke is observed. This behavior affects the weight percentage of coke amount on catalyst, with an antagonistic behavior in the simulations. In case 1 it is observed a higher percentage of coke near the wall and a homogeneous percentage of coke in the other regions, while for case 2, the lower percentage of coke in relation the catalyst occurs near the wall and an increase in percentage toward the center is observed. The behavior observed in case 2

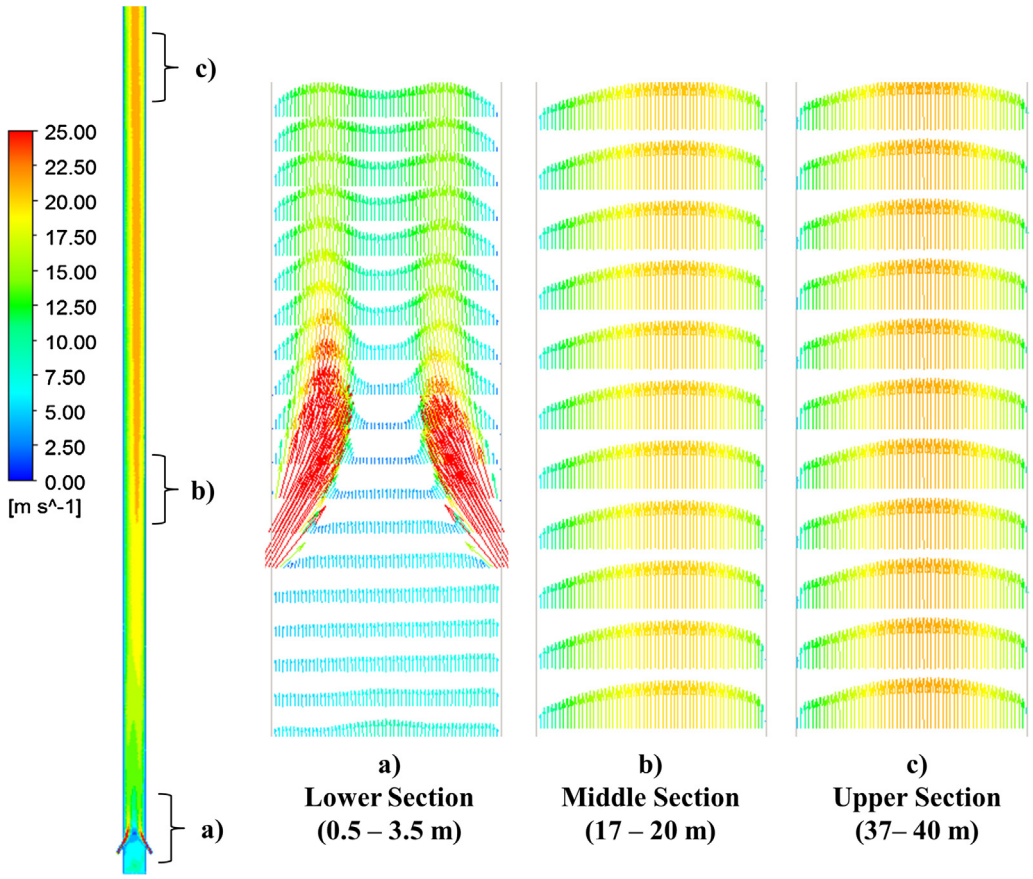

Fig. 4. Velocity profile in axial plane and velocity vector in different heights.

can be attributed to the fact that the mass flow of coke is uniform, thus the regions with low concentration of solid presented a higher percentage of coke amount on catalyst. Furthermore, it can be observed a lower variation in the percentage of coke from the wall to the center of the riser in case 1 and it can be observed that there is a higher area with high weight percentage of the coke amount on catalyst in case 2 . It should be noted that the residence time of the coke in the riser is equal to that of the phase it is produced.

4.4.2. Effect of different treatment for coke with catalyst deactivation as function of residence time

The predicted values of product compositions at the outlet of riser for cases 1 and 2, and the industrial data reported by Chang et al.[3] are listed in Table 6. It can be seen that values predicted in both cases are reasonably in agreement with the industrial data, with the relative errors below 10%, in general. These values of relative errors are acceptable for FCC process [3,7]. It can be seen that the application of novel treatment for coke component had not significant effect on the product compositions when compared with common treatment. This result can be attributed to the fact that the kinetic model used does not depend on the coke distribution, which depends on the temperature, the catalyst distribution and the catalyst residence time.

4.4.3. Effect of different treatment for coke with catalyst deactivation as function of weight percentage of coke

The catalyst deactivation in real FCC process occurs as a function of the coke deposition in catalyst surface, thus the catalyst deactivation as a function of the residence time of the catalyst was replaced by the model in function of the weight percentage of coke amount on catalyst. The simulation results of case 3 and 4 were compared with the industrial results, as shown in Table 7. It can be seen that the values predicted for case 3 and 4 with deactivation model in function of weight percentage of coke are reasonably in agreement with the industrial data. However, in these cases, the treatment for coke component plays a significant role in products composition, mainly in unconverted feedstock, diesel, gasoline, and coke. As discussed and observed in Fig. 7, the treatment for the coke component affects the distribution of coke, thus the different results of cases 3 and 4 may be attributed to that. As it was shown in Fig. 7, in simulation, in which coke is produced in gas phase, there is a higher percentage area with high weight percentage of the coke, consequently a lower conversion was observed in this case.

In Fig. 8 the percentage of coke on the catalyst, the reaction rate of Saturates in feedstock (Ss) and the reaction rate of Aromatics in feedstock (Sa) in cross-sectional planes at different heights are shown in Cases 3 and 4. As mentioned, for the simulation in which the coke is formed in the gas phase (case 4), the mass flow of coke is uniform (Fig. 7), since the coke component diffuses in the gas phase and follows the rate of mixing. For the simulation in which coke is formed in the solid phase (case 3), coke has a flow profile equal to that of the solid. Due to this, the coke percentage for case 4 presents low values close to the wall and high values in the center, while case 3 presents higher values near the wall. We observed in Fig. 8(a) that this behavior extends along the riser for both cases. For case 3, we observed that the difference in the percentage of coke from the wall to the center of the riser decreases along the height. This behavior can be attributed to the fact that the riser operates in pseudo-stationary regime, so part of the solids present near the wall are directed to the center of the riser and vice versa. For case 4, we noted that the difference only tends to increase,

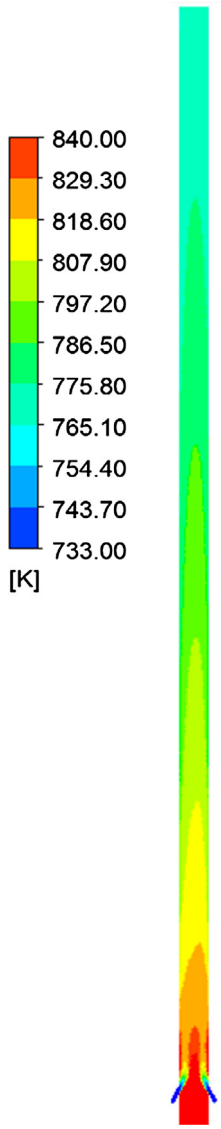

Fig. 5. Contour of gas phase temperature profile.

since the coke flow increases along the height, whereas the flow profile of the catalyst does not show significant change from 10 m in height (Fig. 3).

The distribution effects of the coke percentage on the catalyst, both in the reaction rate profile of Saturates and Aromatics in feedstock along the riser, are shown in Fig. 8(b) and (c). The reaction rate depends on the amount of catalyst present, thus, the region near the wall presents a high reaction rate for both cases. However, case 4 shows a reaction rate near the wall greater than case 3, due to the lower percentage of coke in relation to the catalyst found for case 4. Thus, the catalyst activity near the wall for this case is higher than that for case 3. The opposite occurs in the central region. Case 3 shows a higher rate of reactions than case 4 due to the lower percentage of coke. We also noted that in case 4 the difference in reaction rate from the wall to the center increases along the height, whereas for case 3 it tends to equalize.

The catalytic reactions occurring within the riser are endothermic, thus the temperature in the riser varies with the reaction rates, as show in Fig. 5. In Fig. 9, the temperature in cross-sectional planes at different heights are shown for cases 3 and 4. We noted that the treatment of coke also affects the temperature profile, which is affected by the reaction rates. We observed that for both cases the temperature close to the wall is higher than the temperature in the center; however, the case 4 has a lower temperature near the wall than case 3 due to the higher reaction rates. The reaction rate depends on the catalyst fraction, the percentage of coke on the catalyst and the temperature. In this context, it is noteworthy that the change in the coke distribution altered the profile of the reaction rate in the radial direction and, consequently, the temperature profile, and the temperature also affects the reaction rate. Thus, we noted that the change in one of the variables of the reaction rate affects this directly and indirectly, since these variables also depend on the reaction rate.

4.5. Comparison between deactivation functions

Fig. 10 plots the mass fractions of saturates in feedstock, diesel, olefins in gasoline and coke along the riser height for case 1 (deactivation by residence time) and case 3 (deactivation by percentage of coke). It can be seen that the behavior of the products along the height are similar for two deactivation model, nevertheless a slightly greater difference can be observed in the upper section of the riser.

In Fig. 11 it is plotted the residence time and percentage of coke on catalyst along the riser height. It can be observed that the catalyst residence time increases linearly from 5 m in height, while the weight percentage of coke presents a logarithmic behavior up to a height of approximately 20 m and above that, a linear behavior. In the first half of the riser, it can be seen that the percentage of coke has a higher rate of increase than that of residence time and in the second half of the riser this behavior is reversed. As seen in Fig. 4 and Fig. 5, the velocity and the temperature quickly increases and decreases, respectively, in the first meters of the riser and then do not have major changes from the middle to the upper section. Thus the time function is a linear relationship between distance and velocity, and only increases with the height, while the production of the coke is an exponential function of temperature and catalyst deactivation, that decreases with the height.

The values of catalyst residence time and weight percentage of coke on catalyst of Fig. 11 were applied in their respectively deactivation equations, shown in Fig. 12. It can be observed that up to a height of approximately 23 m, the deactivation functions have a similar deactivation rate. From the height of 23 m, it is noted that the catalyst deactivation as a function of percentage of coke has a reduction in the deactivation rate due to the reduction in the rate of coke formation, whereas the catalyst deactivation as a function of the time has a constant rate of growth.

5. Conclusion

In this work, a 3D CFD model coupled 12-lumps kinetic model was used to describe the hydrodynamic and heterogeneous catalytic cracking reactions in FCC riser. The coke deposition on the catalyst phase was included in the mathematical model and it was compared with traditional treatment, in which coke is produced in gas phase. It was proposed a catalyst deactivation model as a function of the weight percentage of coke on catalyst to replace the deactivation model as function of the catalyst residence time. Both models showed good agreement with industrial data.

The results showed that treatment for coke component plays an important role in radial distribution of coke mass flow and consequently radial distribution of percentage of coke on catalyst. The treatment, in which coke is produced in catalyst phase, presented hydrodynamic results closer to the expected. Furthermore, the results indicated that the treatment for coke have a significant influence on products yield in simulation with catalyst deactiva-

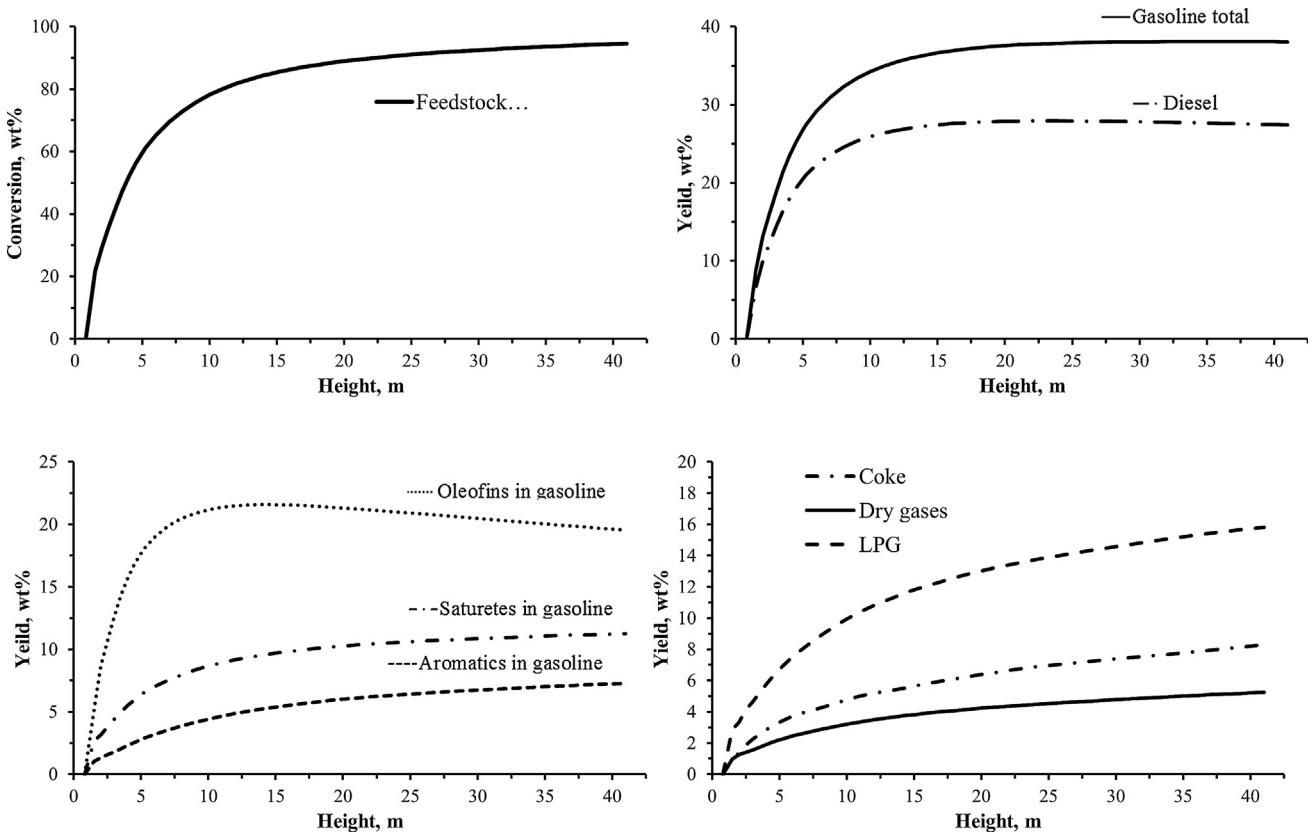

Fig. 6. Feedstock conversion and species concentrations.

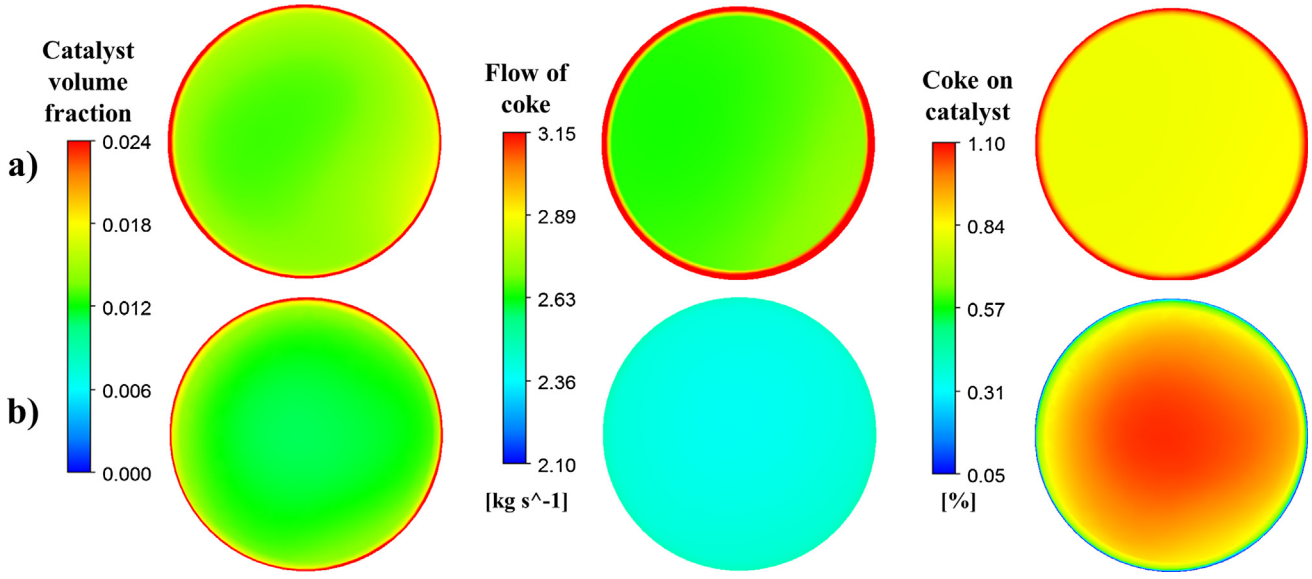

Fig. 7. Catalyst volume fraction, coke mass flow and weight percentage of coke on catalyst in cross section planes at 25 m. (a) Case 1 and (b) Case 2.

tion as function of the mass fraction of coke deposited on catalysts, while it was not observed significant effects on products yield in simulation with catalyst deactivation as function of residence time.

The deactivation model as function of the coke presented a behavior of the catalyst activity over time that is closer to that expected in reality, which presents a reduction in the deactivation rate over time, since the coke production rate is reduced. Nevertheless, deactivation model as a function of residence time had a constant increase in the deactivation rate. Thus, in studies, where the residence time is sufficiently long, the time-based deactivation model may present an exacerbated reduction in catalyst activity.

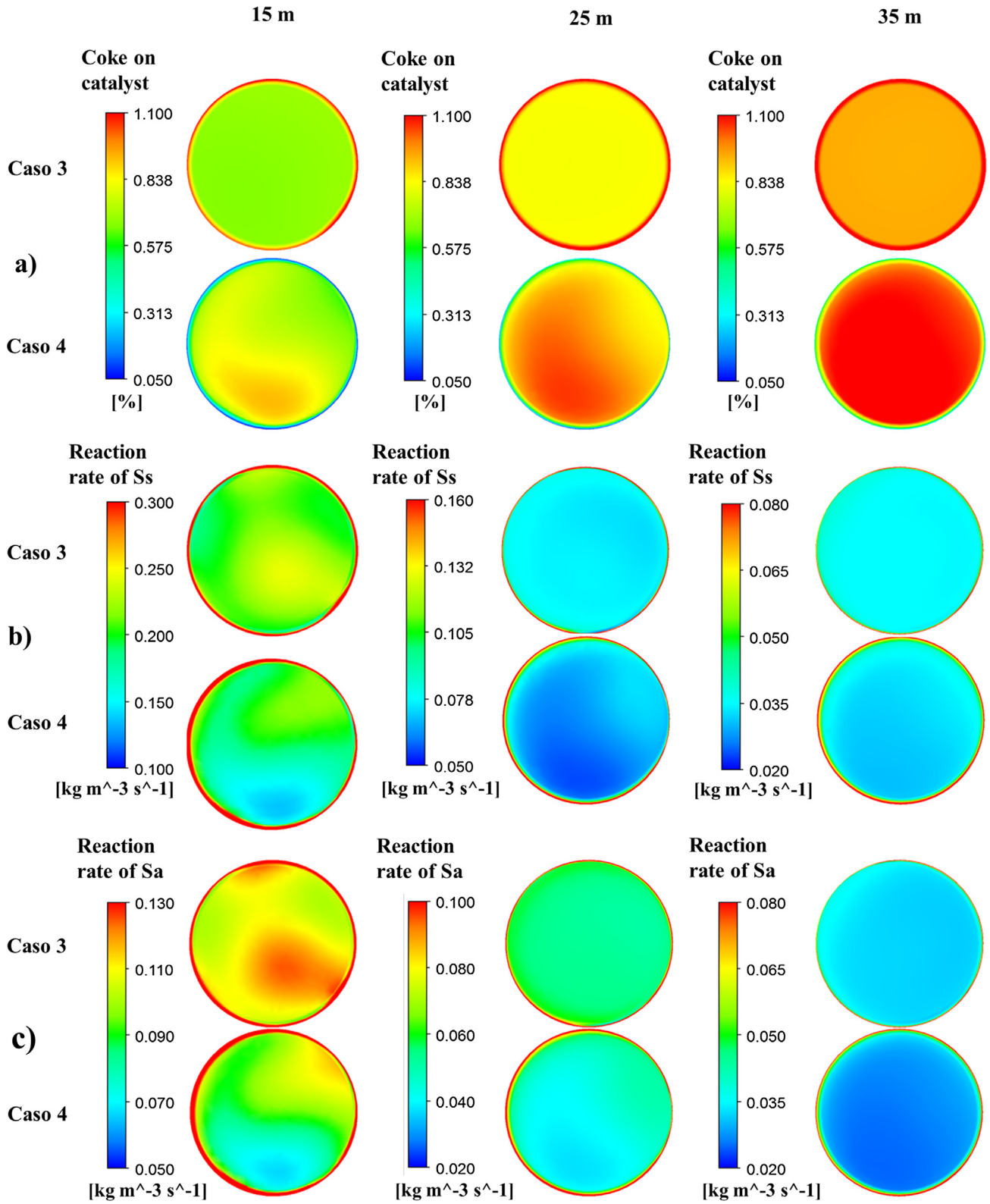

Fig. 8. Profiles in radial planes for Case 3 and Case 4 in different heights for (a) weight percentage of coke on catalyst, (b) reaction rate of saturates in feedstock (S_S) and (c) reaction rate of aromatics in feedstock (S_A).

Table 6
Comparison between simulated results and industrial data.

	Industrial data	Numerical result		Relative error (%)	
		Case 1	Case 2	Case 1	Case 2
Gas velocity at riser outlet (m/s)	12–18	16.22	16.36	–	–
Temperature at riser outlet (K)	793.15	770.19	769.67	−2.89	−2.96
Unconverted feedstock	4.92	5.36	5.46	8.94	10.98
Saturates	1.09	1.61	1.65	47.71	51.38
Aromatics	2.94	2.82	2.87	−4.08	−2.38
Resin and Asphaltene	0.89	0.93	0.94	4.49	5.62
Diesel	27.45	27.34	27.36	−0.40	−0.33
Gasoline	39.29	37.95	37.94	−3.41	−3.44
Saturates	11.23	11.22	11.18	−0.09	−0.45
Oleofin	20.2	19.48	19.55	−3.56	−3.22
Aromatics	7.86	7.25	7.21	−7.76	−8.27
LPG	15.33	15.79	15.65	3.00	2.09
Low carbon alkanes	4.82	4.78	4.75	−0.83	−1.45
Propylene	5.42	5.39	5.35	−0.55	−1.29
Butene	5.09	5.62	5.55	10.41	9.04
Dry gases	4.75	5.23	5.18	10.11	9.05
Coke	8.26	8.33	8.41	0.85	1.82

Table 7
Comparison between simulated results and industrial data.

	Industrial data	Numerical result		Relative error (%)	
		Case 3	Case 4	Case 3	Case 4
Gas velocity at riser outlet (m/s)	12–18	16.38	16.50	–	–
Temperature at riser outlet (K)	793.15	768.14	768.06	−3.15	−3.16
Unconverted feedstock	4.92	4.59	5.08	−6.71	3.25
Saturates	1.09	1.27	1.53	16.51	40.37
Aromatics	2.94	2.5	2.67	−14.97	−9.18
Resin and Asphaltene	0.89	0.82	0.88	−7.87	−1.12
Diesel	27.45	27.23	26.77	−0.80	−2.48
Gasoline	39.29	38.01	37.46	−3.26	−4.66
Saturates	11.23	11.39	11.25	1.42	0.18
Oleofin	20.2	19.15	18.9	−5.20	−6.44
Aromatics	7.86	7.47	7.31	−4.96	−7.00
LPG	15.33	16.27	16.34	6.13	6.59
Low carbon alkanes	4.82	4.87	4.84	1.04	0.41
Propylene	5.42	5.55	5.54	2.40	2.21
Butene	5.09	5.85	5.96	14.93	17.09
Dry gases	4.75	5.41	5.47	13.89	15.16
Coke	8.26	8.48	8.89	2.66	7.63

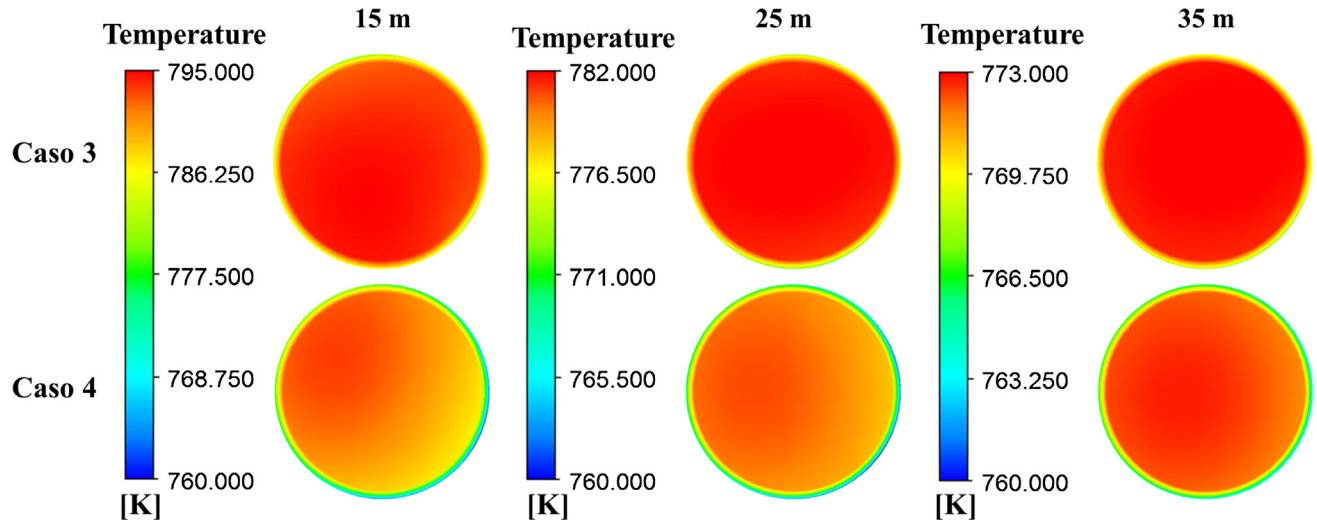

Fig. 9. Temperature profile in cross section planes for Case 3 and Case 4 in different heights.

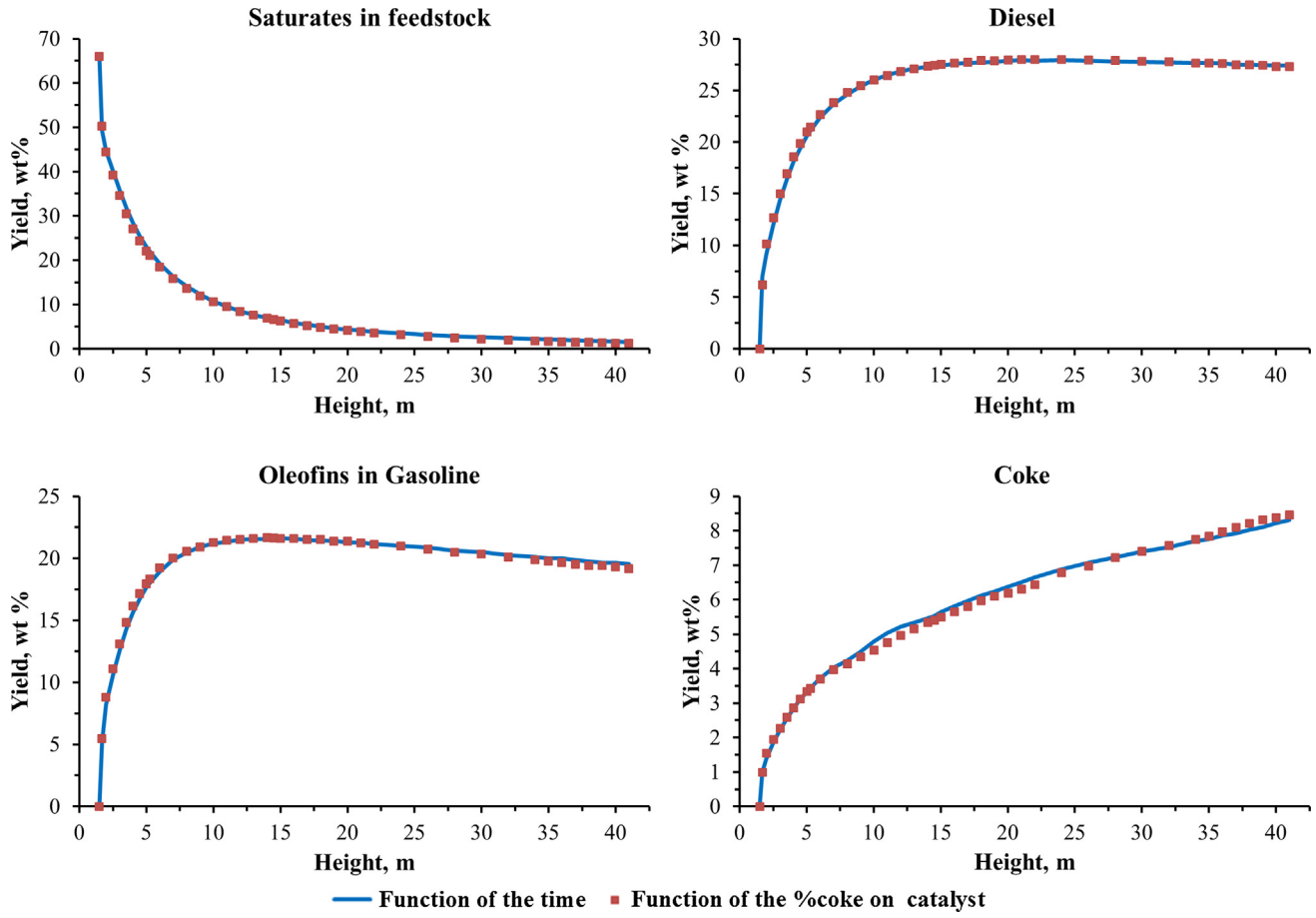

Fig. 10. Yield of saturates in feedstock, diesel, olefins in gasoline and coke.

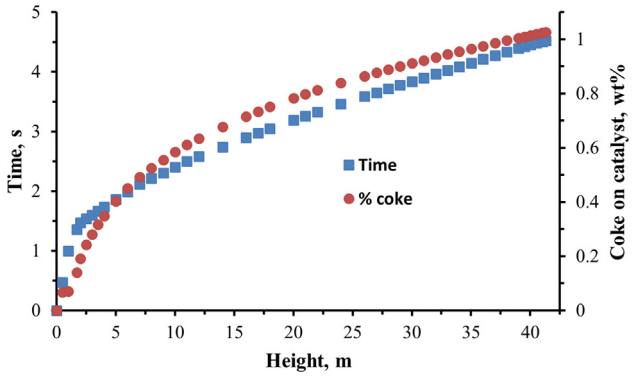

Fig. 11. Catalyst residence time and weight percentage of coke on catalyst.

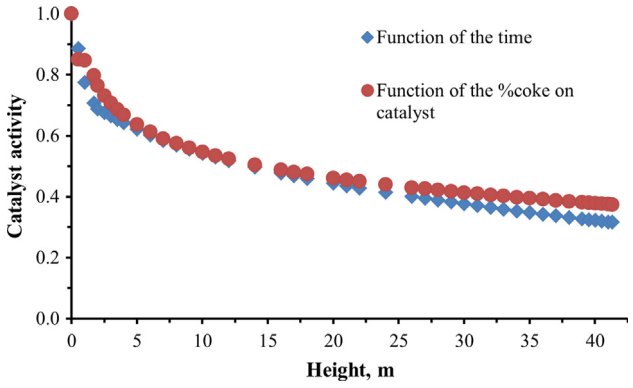

Fig. 12. Catalyst activity as functions of residence time and percentage of coke on catalyst.

Acknowledgement

The authors are grateful for financial support from Petrobras and CAPES. The authors thank "Espaço da Escrita – Coordenadoria Geral da Universidade – UNICAMP" for the language services provided.

References

[1] H. Gao, G. Gang, R. Li, C. Xu, J. Gao, Study on the catalytic cracking of heavy oil by proper cut for higher conversion and desirable products, Energy & Fuels 26 (2012) 1880–1891.
[2] C.I.C. Pinheiro, J.L. Fernandes, L. Domingues, L.J.J. Chambel, I. Graça, N.M.C. Oliveira, H.S. Cequeira, F.R. Ribeiro, Fluid catalytic cracking (FCC) process modeling, simulation and control, Ind. Eng. Chem. Res. 51 (2012) 1–29.

[3] J. Chang, F. Meng, L. Wang, K. Zhang, H. Chen, Y. Yang, CFD investigation of hydrodynamics, heat transfer and cracking reaction in a heavy oil riser with bottom airlift loop mixer, Chem. Eng. Sci. 78 (2012) 128–143.
[4] H.C. Alvarez-Castro, E.M. Matos, M. Mori, W. Martignoni, R. Ocone, Analysis of process variables via CFD to evaluate the performance of a FCC riser, Int. J. Chem. Eng. (2015) 1–13.
[5] Y.E.C. Fan, M. Shi, C. Xu, J. Gao, C. Lu, Diffusion of feed spray in fluid catalytic cracking, AIChE J. 56 (2010) 858–868.
[6] M.A. Fahim, T.A. Alsahhaf, A.S. Elkilani, Chapter 8 – Fluidized Catalytic Cracking, in: Fundamentals of Petroleum Refining, Elsevier, Amsterdam, 2010, pp. 199–235.
[7] Q. Yang, A.S. Berrouk, Y. Du, H. Zhao, C. Yang, M.A. Rakib, A. Mohamed, A. Taher, CFD investigation of hydrodynamics, heat transfer and cracking reactions in a large-scale fluidized catalytic cracking riser, Appl. Math. Model. (2016) 1–20.
[8] K.N. Theologos, I.D. Nikou, A.I. Lygeros, N.C. Markatos, Simulation and design of fluid catalytic cracking riser-type reactors, Comp. Chem. Eng. 20 (1997) 757–762.
[9] G.C. Lopes, L.M. Rosa, M. Mori, J.R. Nunhez, W.P. Martignoni, CFD study of industrial FCC risers: the effect of configurations on hydrodynamics and reactions, Int. J. Chem. Eng. 2012 (2012) 1–16.
[10] Y. Behjat, S. Shahhosseini, M.A. Marvast, Modeling gas oil spray coalescence and vaporization in gas solid riser reactor, Int. Comm. Heat Mass Transf. 37 (2010) 935–943.
[11] J. Li, Y.P. Fan, C.X. Lu, Z.H. Luo, Numerical simulation of influence of feed injection on hydrodynamic behavior and catalytic cracking reactions in a FCC riser under reactive conditions, Ind. Eng. Chem. Res. 52 (2013) 11084–11098.
[12] A.V. Nayak, S.L. Joshi, V.V. Ranade, Modeling of vaporization and cracking of liquid oil injected in a gas-solid riser, Chem. Eng. Sci. 60 (2005) 6049–6066.
[13] V.W.J.R. Weekman, D.M. Nace, Kinetics of catalytic cracking selectivity in fixed, moving and fluid bed reactors, AIChE J. 16 (1970) 397–404.
[14] J.A. Juarez, F.L. Isunza, E.A. Rodriguez, J.C.M. Mayorga, A strategy for kinetic parameter estimation in the fluid catalytic cracking process, Ind. Eng. Chem. Res. 36 (1997) 5170–5174.
[15] K. Xiong, C. Lu, Z. Wang, X. Gao, Quantitative correlations of cracking performance with physiochemical properties of FCC catalysts by novel lump kinetic modelling method, Fuel 161 (2015) 113–119.
[16] P.K. Dasila, I.R. Choudhury, S. Singh, S. Rajagopal, S.J. Chopra, D.N. Saraf, Simulation of an industrial fluid catalytic cracking riser reactor using a novel 10-lump kinetic model and some parametric sensitivity studies, Ind. Eng. Chem. Res. 53 (2014) 19660–19670.
[17] O. Fousheng, X. Qihong, N. Hui, A kinetic model for flexible dual-riser fluid catalytic cracking process, Pet. Sci. and Technol. 33 (2015) 614–621.
[18] X. Lan, C. Xu, G. Wang, L. Wu, J. Gao, CFD modeling of gas-solid flow and cracking reaction in two-stage riser FCC reactors, Chem. Eng. Sci. 64 (2009) 3847–3858.
[19] H.S. Cerqueira, E.C. Biscaia Jr, E.F.S. Aguiar, Mathematical modeling of deactivation by coke formation in the cracking of gasoil, Cat. Deac. 111 (1997) 303–310.
[20] M. Guisnet, F.R. Ribeiro, Chapter 9 – deactivation and regeneration of zelite catalysts, Cat. Sci. Series 9 (2011) 151–169.
[21] F.Y. Wu, H.X. Weng, Establishment of combined model for lumped reaction kinetics of FDFCC, J. East China Univ. Sci. Technol. 35 (2009) 350–356.
[22] J. Gan, H. Zhao, A.S. Berrouk, C. Yang, H. Shan, H, Numerical simulation of hydrodynamics and cracking reactions in the feed mixing zone of a multiregime gas-solid riser reactor, Ind. Eng. Chem. Res. 50 (2011) 11511–11520.
[23] D. Gidaspow, Multiphase Flow and Fluidization: Continuum and Kinetic Theory Descriptions, Academic Press, San Diego, 1994.
[24] M. Syamlal, T.J. O'brien, Computer simulation of bubbles in fluidized bed, AIChE Symp. 85 (1989) 22–31.
[25] N. Yang, W. Wang, W. Ge, J. Li, CFD simulations of concurrent up gas solid flow in CFB structure dependent drag coefficient, Chem. Eng. J. 96 (2003) 71–80.
[26] W.E. Ranz, W.R. Marshall, Evaporation from drops, Part I, Chem. Eng. Prog. 48 (1952) 173–180.
[27] W.E. Ranz, W.R. Marshall, Evaporation from drops, Part II, Chem. Eng. Prog. 48 (1952) 173–180.
[28] A. Hany, R. Sohrab, Dynamic modelling and simulation of a riser type fluid catalytic cracking unit, Chem. Eng. Technol. 20 (1997) 118–130.
[29] Y.G. Bolkan-Kenny, T.S. Pugsley, F. Berruti, Computer simulation of the performance of fluid catalytic cracking riser and dowers, Ind. Eng. Chem. Res. 33 (1994) 3043–3052.
[30] G.C. Lopes, Computational Study of the Dynamic of the Reactive Flow in FCC Industrial Risers, University of Campinas, Campinas, Brazil, 2012 (Phd Thesis).
[31] H.C. Alvarez-Castro, E.M. Matos, M. Mori, W. Martignoni, R. Ocone, The influence of the fluidization velocities on product yield and catalyst residence time in industrial risers, Adv. Powder Technol. 26 (2015) 836–847.